Inference for point processes with unobserved one-dimensional reference structure

J. Su, B. Hill, W.S. Kendall and E. Thönnes

June 18, 2008

Abstract

We present a novel approach to examining local anisotropy in planar point processes. Our method is based on a kernel Principal Component Analysis and produces a tensor field that describes local orientation. The approach is illustrated on an example examining pore patterns in ink fingerprints.

KEYWORDS: Fingerprint, pore pattern, point process, directional analysis, local anisotropy, kernel PCA, tensor field, Rice formula

1 Introduction

In this paper we consider planar point processes that are observed on a (random) reference set. We develop an approach that infers the local orientation of the reference set which can then be used to explore some of its geometrical and topological characteristics. As an example, we consider sweat pore features in fingerprints. Sweat pores lie on the ridges of the palmar skin of humans. Solely based on the location of sweat pores we infer the local orientation of the ridge structure. This information produces an orientation field that enables tasks such as fingerprint classification, registration of fingerprint images using warping and classification of pores according to ridge association.

Fingerprints have been used as a tool for identification since the early twentieth century [2]. They are produced by friction ridge skin whose general topology can be classified into a small number of standard patterns. Figure 1(a) shows an example ink fingerprint, whose general pattern is called a loop. The ridge flow exhibits isolated singularities such as ridge endings and bifurcations. These are called minutiae or level two features and are commonly used for identification and verification. However, with the improvement of imaging technology, and availability of storage, the interest is moving towards using finer detail features. So called level three features include ridge shape, sweat pore shape and sweat pore location. In [8] first steps towards quantifying evidence of sweat pore locations are discussed. Sweat pores are more densely distributed on fingerprints than minutiae and so pore patterns seem a viable alternative for identification.

While spatial models have been proposed for minutiae pattern [2], but very little attempts have been made to investigate the relation between pores and the underlying ridge structure. In this paper we begin to address this question

by considering a fundamental issue: how much information does a (noisy) pore pattern reveal about the underlying ridge structure?

2 Data

To illustrate our method we use an ink fingerprint from the NIST 30 special database [18]. We examine a central 256×256 pixel section from fingerprint 'a002_05', see Figure 1(a), which was scanned at a resolution of 500 dpi. To extract the pore pattern from the fingerprint image we use the following algorithm, a simpler version of the algorithm in [6]. For an alternative algorithm see [8]. As a first step the image is normalized to have zero mean and unit variance. The aim of this normalization is to reduce the variations in grey level values along the ridges and furrows. All subsequent procedures take place on the normalized image. In order to enhance the pores in the image we use a 2D Mexican hat wavelet transform which is a bandpass filter that captures the high negative frequency response at the location of pores. The 2D Mexican hat wavelet with scale s is given by

$$\phi(x,y) \quad = \quad \Big((\frac{x}{s})^2 + (\frac{y}{s})^2 - 2\Big) \exp\Big(-\frac{1}{2}(\frac{x}{s})^2 + (\frac{y}{s})^2\Big)$$

and is convolved with the image. The filter response then is normalized using a min-max normalization. To extract the pores we identify the regional minima in the filtered image using the H-transform with a depth threshold of t_1. Any regional minima whose area is greater than t_2 is removed. We then determine the pore locations as the centroids of the regional minima. For the print in Figure 1(a) we used parameters $s = 0.7, t_1 = 0.15$ and $t_2 = 15$. Figure 1(b) shows the extracted pore locations on the right.

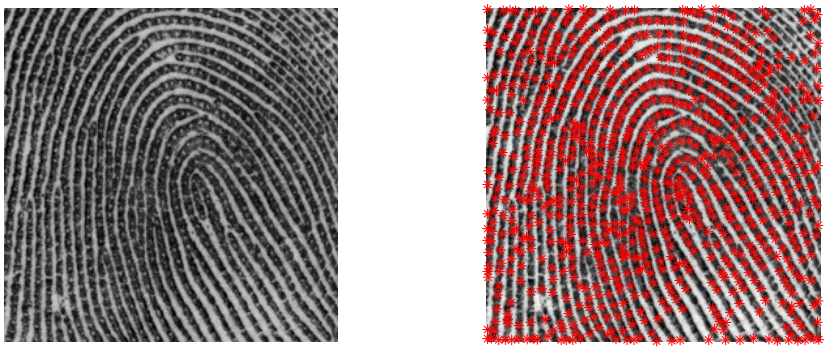

(a) Original fingerprint section.

(b) Extracted pore locations.

Figure 1: Fingerprint a002_05.

3 Methods for the analysis of anisotropy in point patterns

The directional analysis of point processes was developed in papers such as [9, 14, 15]. We follow the description in [16]. The directional distribution $\Theta_{r1,r2}$ of a point process Φ is the distribution function (or rose) of the directions of segments formed by point pairs of the point process whose inter-point distances lie between r_1 and r_2. Anisotropy is indicated by departure of Θ_{r_1,r_2} from uniformity. Related to Θ_{r_1,r_2} is the rose density which is simply the density of the distribution function Θ_{r_1,r_2}. To estimate the rose density kernel density estimation methods are used.

The method above investigates (scale-dependent) global directionality over the whole point pattern. In contrast we are interested in local directionality, which can then be extrapolated to an orientation field over the whole sampling window. While the method above could be easily generalized to our aim of estimating local directionality by applying appropriate windowing functions, this would be a computationally rather expensive approach. The rose of direction was developed as a tool to quantify departure from isotropy rather than estimating the orientation per se. To produce an orientation estimate the modes of the rose density need to be determined which is computationally much more expensive than our approach.

4 Estimation of local ridge structure

We will describe the local ridge orientation by the orientation of the dominant eigenvector field of a tensor field $S(x)$ where $x \in W$. Here W is the sampling window in which the fingerprint is observed. In the following we identify tensors with 2×2 symmetric, positive definite matrices. To obtain the tensor field we first estimate the tensors at the pore locations. Tensor estimates at other locations in W can then be produced by interpolation, see Section 5.

To produce a local orientation estimate we will use a Principal Component Analysis (PCA). The orientation of the first principal component then can be used as an orientation estimate for the anisotropic point cloud. However, as we are trying to estimate *local* orientation properties, it is immediately clear that nearby pores should be given a larger weight than pores at larger distance from the location of interest. To do this we use a kernel-based Principle Component Analysis (KPCA) [13]. KPCA is a computationally efficient form of non-linear PCA which uses a non-linear transformation from the space of the data to a possibly higher-dimensional feature space. In our example we use a Gaussian kernel with standard deviation σ. This has the advantage that the influence of pore locations further than a distance of $2\,\sigma$ from the location of interest is very limited, see also Section 6.

In more detail, suppose the pore pattern has n pores at locations $\{x_1, \ldots, x_n\}$. Let x_n be the location at which we estimate the tensor. We assume without loss of generality that $x_n = \mathbf{0}$ is the origin and then apply a non-linear transformation ϕ to the pore pattern. Let $\{(R_1, \theta_1), \ldots, (R_{n-1}, \theta_{n-1})\}$ be the polar coordinates of the pore locations $\{x_1, \ldots, x_{n-1}\}$. We map the pore at location

(R_i, θ_i) to the location $(\tilde{R}_i, \theta_i)$ where

$$\tilde{R}_i \quad = \quad \exp\Big(-\frac{1}{2\sigma^2}R_i^2\Big) \qquad \text{for } i = 1, \ldots, n-1.$$

Thus $\phi : R_0^+ \times [0, \pi] \to [0, 1] \times [0, \pi]$ with

$$\phi(R, \theta) \quad = \quad \Big(\exp\Big[-\frac{1}{2\sigma^2}R_i^2\Big], \theta\Big).$$

Let

$$\Phi^+ \quad = \quad \{(\tilde{R}_1 \cos(\theta_1), \tilde{R}_1 \sin(\theta_1)), \ldots, (\tilde{R}_{n-1} \cos(\theta_{n-1})), \tilde{R}_{n-1} \sin(\theta_{n-1}))\}$$

be the transformed pore pattern. Then define

$$\Phi^- = \{(-\tilde{R}_1 \cos(\theta_1), -\tilde{R}_1 \sin(\theta_1)), \ldots, (-\tilde{R}_{n-1} \cos(\theta_{n-1})), -\tilde{R}_{n-1} \sin(\theta_{n-1}))\}$$

as the point pattern produced by rotating Φ^+ by 180^0 around the origin.

The estimate of the tensor at location x_n is then given by $S(x_n) = \Sigma$ where Σ is the variance-covariance matrix of $\Phi = \Phi^+ \cup \Phi^-$. The local orientation estimate at x_n is given by the orientation of the major eigenvector of $S(x_n)$ (or first principal component of Φ). Figure 2(a) shows the orientation of the major eigenvectors at the pore locations for the fingerprint in Figure 1(a). For this example the smoothing parameter σ was chosen to be equal to 10.

Let $\lambda_1(x_n)$ and $\lambda_2(x_n)$ be the eigenvalues of the major and minor eigenvector of $S(x_n)$ respectively. The fractional anisotropy index

$$\text{FAI}(x_n) \quad = \quad \frac{\lambda_1(x_n)}{\lambda_1(x_n) + \lambda_2(x_n)} \quad \in \quad [\frac{1}{2}, 1]$$

gives a measure of accuracy of the orientation estimate. A large FAI indicates strong evidence for the estimated local orientation.

5 Interpolation of tensors

To obtain tensor estimates at arbitrary locations x within the sampling window we use interpolation based on a Gaussian kernel. This also induces smoothing. A naive approach to interpolating tensors would be based on the Frobenius norm to define a distance measure. This yields a Euclidean structure that allows for cheap computation of Euclidean means. While this approach yielded acceptable results in our experiments, it has the undesirable effect of "tensor swelling" [1]: the determinant of a tensor average can be larger than the determinant of the original tensors. Furthermore, tensor averages may have null or negative eigenvalues. Affine-invariant Riemannian metrics [4] avoid this problem but are computationally expensive. An alternative is proposed in [1] using the so-called Log-Euclidean metric. This method is based on performing Euclidean computations on the matrix logarithm of the tensors. A Log-Euclidean weighted average of a set of tensors $S_1, \ldots, S_N$ is defined as

$$\bar{S} \quad = \quad \exp\Big(\sum_{i=1}^{N} w_i \log(S_i)\Big)$$

where $\log(S_i)$ is the logarithm of the matrix S_i and w_i is the chosen weight. Hence this is a generalization of the geometric mean. Because the mean is based on the Euclidean operations and matrix exponentials and logarithms it is relatively cheap to compute. Figure 2(b) shows the direction of the major eigenvector field derived from the tensor field interpolation.

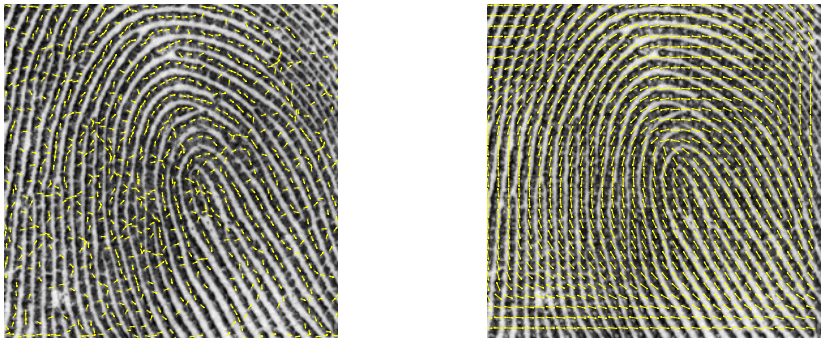

(a) Major eigenvectors at pore locations. (b) Major eigenvectors on a regular grid.

Figure 2: Major eigenvectors of the estimated tensor field for fingerprint a002_05.

Using the above interpolation method, we can then use methods such as the Runge-Kutta algorithm [10] to produce streamlines that illustrate the general topology of the ridge flow.

6 The smoothing parameter σ

The method presented in Section 4 derives an orientation estimate at x_n by examining the orientations θ_j of line segments between x_n and x_j where $j \in \{1, \ldots, n-1\}$. The influence of a pore location x_k on the orientation estimate can be bounded in terms of its distance R_k from x_n as the following calculations show.

Set $\Sigma = (n-1)S(x_n)$ where $S(x_n)$ is the tensor estimate at x_n. Suppose we remove the pore location x_1 and consider the tensor estimate $\tilde{S}(x_n)$ based on the pore locations $\{x_2, \ldots, x_n\}$. Let θ_1 be the orientation of the line segment connecting x_1 with x_n and $d_1 = \exp(-R_1^2/\sigma^2)$. Set $\tilde{\Sigma} = (n-2)\tilde{S}(x_n)$ and consider the matrix $\delta\Sigma$ defined as

$$\delta\Sigma \quad := \quad \Sigma - \tilde{\Sigma} \; = \; \begin{pmatrix} 2d_1\cos^2(\theta_1) & 2d_1\cos(\theta_1)\sin(\theta_1) \\ 2d_1\cos(\theta_1)\sin(\theta_1) & 2d_1\sin^2(\theta_1) \end{pmatrix}.$$

Using the Frobenius norm to define a distance measure between Σ and $\tilde{\Sigma}$ we

have

$$\begin{aligned} d(\Sigma, \tilde{\Sigma}) &= \sqrt{\text{trace}\Big(\delta\Sigma\Big)^2} \\ &= d_1\sqrt{\cos^2(\theta_1) + \sin^2(\theta_1)} \quad = \quad d_1. \end{aligned}$$

The above shows that the further a pore location is from x_n the less influence it has on the principal eigenvector of the tensor estimate at x_n. The rate at which this influence reduces is dependent on the smoothing parameter σ.

More specifically, we can use eigenvector perturbation theory to bound the influence of the pore location x_1 on the orientation of the major eigenvector of $S(x_n)$. A more general version of the following theorem and corollary is derived in [7]:

Theorem 1 *Let Σ and $\tilde{\Sigma}$ be symmetric, positive definite 2-by-2 matrices with their respective eigendecompositions:*

$$\Sigma \quad = \quad U\Lambda U^T \quad \textit{and} \quad \tilde{\Sigma} \quad = \quad V\Gamma V^T.$$

where $\Lambda = diag(\lambda_1, \lambda_2)$ and $\Gamma = \text{diag}(\gamma_1, \gamma_2)$. Assume $\tilde{\Sigma} = \Sigma + \delta\Sigma$ and set $S = U^T V$. Further assume that $\lambda_1 \leq \lambda_2$ and $\gamma_1 \leq \gamma_2$. If

$$\eta \quad = \quad ||\Sigma^{-\frac{1}{2}}\delta\Sigma\Sigma^{-\frac{1}{2}}|| \quad < \quad 1$$

then the elements of S are bounded by

$$|s_{ij}| \quad \leq \quad \frac{\sqrt{\lambda_i\gamma_j}}{|\lambda_i - \gamma_j|}\frac{\eta}{\sqrt{1-\eta}} \qquad i, j \in \{1, 2\}.$$

The above theorem together with the fact that

$$\lambda_i(1-\eta) \quad \leq \quad \gamma_i \quad \leq \quad \lambda_i(1+\eta)$$

implies the following corollary.

Corollary 1 *Under the assumption of Theorem 1 let u_1 and v_1 be the major eigenvectors of Σ and $\tilde{\Sigma}$ respectively, then*

$$||v_1 - u_1|| \quad \leq \quad \frac{\sqrt{2}\eta}{\sqrt{1-\eta}}\frac{\sqrt{\lambda_1\gamma_2}}{|\lambda_1 - \gamma_2|} \quad < \quad \sqrt{2}\frac{\eta}{(1-\eta)}\frac{\sqrt{\gamma_1\gamma_2}}{\gamma_1 - \gamma_2}.$$

Let us examine η in our setting. As before we have $\Sigma = (n-1)S(x_n)$, based on the full point pattern, and $\tilde{\Sigma} = (n-2)\tilde{S}(x_n)$, produced by removing the pore at location x_1. Set $D = \sqrt{\text{diag}(\Sigma)}$ and $A = D^{-1}\Sigma D^{-1}$. Then it can be shown [17] that

$$\eta \quad \leq \quad \sqrt{2}\kappa(A)\epsilon \quad \leq \quad \sqrt{8}\epsilon\frac{\lambda_1}{\lambda_2}$$

where $\kappa(A)$ is the condition number of A and $\epsilon > 0$ is such that

$$|\delta\Sigma_{ij}| \quad \leq \quad \epsilon|\Sigma_{ij}|.$$

We have $|\delta\Sigma_{ij}| \leq \exp(-R_1^2/\sigma^2)$ and $|\Sigma_{ij}| \geq \min\{\tilde{\Sigma}_{11}, \tilde{\Sigma}_{22}\}$ and so we can set

$$\epsilon \quad = \quad \exp(-R_1^2/\sigma^2)\max\{\tilde{\Sigma}_{11}^{-1}, \tilde{\Sigma}_{22}^{-1}\}.$$

This again illustrates that for small σ pore locations that lie far from x_n have little influence on the first eigenvector of $S(x_n)$.

To examine the effect of removing more than one pore location we performed the following numerical experiment. When estimating the tensor at a pore location x_n we only consider pores $x_k, \ldots, x_{n-1}$ that lie at a distance less than 2σ units from x_n. Figure 6 shows the major eigenvectors of the tensors derived with this method in yellow and the the ones estimated the full pore pattern in red. As can be seen, the red arrows are almost completely covered by yellow arrows illustrating there is very little difference in the local orientation estimates.

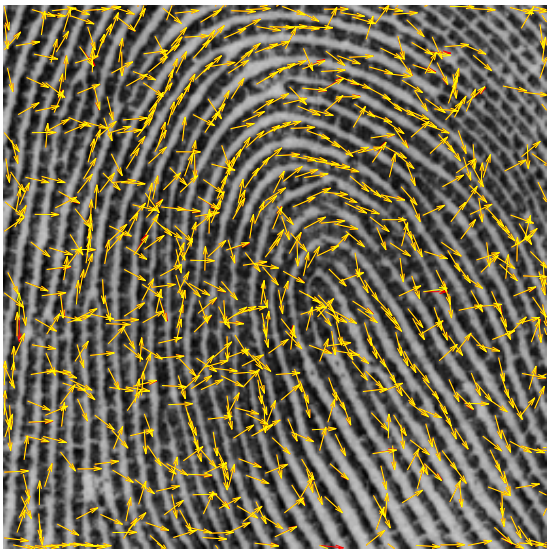

Figure 3: Major eigenvectors of the estimated tensor field for fingerprint a002_05. Red arrows show the the estimates based on the full pore pattern whereas yellow arrows show the the estimates based on the pore pattern within a local 2σ window. There is virtually no difference between the estimates and so the red arrows can hardly be seen.

7 Rice's formula for the expected number of singularities in the random field

The major eigenvector field derived from the tensor field provides estimates of the local ridge flow direction. However, at isolated points within the sampling window the tensor may be such that it has equal eigenvalues. In this case the definition of major versus minor eigenvector is arbitrary. The degenerate points

of a tensor field play an analogous role to critical points in vector fields and so determine the topology of the tensor field. As discussed in [5] the basic patterns at degenerate points are trisectors and wedges. At trisectors three hyperbolic sectors occur where streamlines sweep past the degenerate point. At wedges there is only one hyperbolic sector. Thus, trisectors and wedges correspond roughly to bifurcations and ridge endings. The two types of degenerate points can be distinguished using a tensor index, see [5]. However, in this paper we do not consider this distinction any further.

In the following we model the tensor field as a Gaussian field and derive the expected number of degenerate points. We then compare the theoretically derived number with the manually identified rate of level two features. Recall that for $x \in W$ we have

$$S(x) \quad = \quad \begin{pmatrix} S_{11}(x) & S_{12}(x) \\ S_{21}(x) & S_{22}(x) \end{pmatrix} \quad = \quad \begin{pmatrix} a & c \\ c & b \end{pmatrix} \qquad a, b > 0,\ c \in \mathbb{R},$$

which will have equal eigenvalues if $a = b$ and $c = 0$. We define the random field Z as

$$Z(x) \quad = \quad \begin{pmatrix} Z_1(x) \\ Z_2(x) \end{pmatrix} \quad = \quad \begin{pmatrix} (S_{11}(x) - S_{22}(x))/s_1(x) \\ S_{12}(x)/s_2(x) \end{pmatrix} \qquad x \in W,$$

where $s_1^2(x) = \mathrm{Var}(S_{11}(x) - S_{22}(x))$ and $s_2^2(x) = \mathrm{Var}(S_{12}(x))$.

In order to obtain an indicative result we assume that Z is a smooth, zero mean Gaussian field with independent components that have a Gaussian covariance function, that is

$$\begin{aligned} \mathrm{Cov}\Big(Z_1(x), Z_1(y)\Big) &= \exp\Big(-\frac{1}{2\alpha^2}||x-y||_2^2\Big), \qquad \alpha > 0 \\ \mathrm{Cov}\Big(Z_2(x), Z_2(y)\Big) &= \exp\Big(-\frac{1}{2\beta^2}||x-y||_2^2\Big), \qquad \beta > 0 \\ \mathrm{Cov}\Big(Z_1(x), Z_2(y)\Big) &= 0. \end{aligned}$$

We can now use an extension of Rice's formula to examine the zeros of the Gaussian field Z. Rice's original formula [11, 12] gives an expression for the expected number of upcrossings by a stochastic process $Z(t)$. It provides a formula for a stationary process $Z(t)$ with parameter $t \in \mathbb{R}$. In Theorem 2.1 of [3] the result is extended to $x \in \mathbb{R}^d$ as follows.

Theorem 2 *Let I be an open subset of $\mathbb{R}^d$, let $Z : I \to \mathbb{R}^d$ and let $u \in \mathbb{R}^d$ be a fixed point in the codomain. Let $N_u(B)$ denote the number of roots of the equation $Z(x) = u$ on the Borel set B contained in I. Assume that*

1. *Z is a Gaussian random field;*
2. *$x \to Z(x)$ is almost surely of class $\mathcal{C}^1$.*
3. *For each $x \in I$ the random variable $Z(x)$ has a non-degenerate distribution;*
4. *$\mathbb{P}\Big(\exists x \in I,\ Z(x) = u,\ \det(Z'(x)) = 0\Big) = 0$;*

Then, for every Borel set B in I

$$\mathbb{E}(N_u(B)) \quad = \quad \int_B \mathbb{E}\Big(|\det(Z'(x))|\Big|Z(x)=u\Big)p_{Z(x)}(u)dx,$$

where $p_{Z(x)}$ is the density of $Z(x)$.

Corollary 2 *Additional to the assumptions in Theorem 1, suppose Z is a stationary Gaussian field on $\mathbb{R}^2$, $u=\mathbf{0}$ is the origin in R^2 and $B=[0,1]^2$ is the unit square. Then*

$$E(N_{\mathbf{0}}([0,1]^2)) \quad = \quad p_{Z(\mathbf{0})}(\mathbf{0})\ \mathbb{E}\Big(|\det(Z'\mathbf{0})|\Big|Z(\mathbf{0})=\mathbf{0}\Big).$$

For the random field Z defined earlier we have $p_{Z(\mathbf{0})}(\mathbf{0})=1/(2\pi)$. Furthermore, from the covariance assumptions we can deduce that Z and all partial derivatives at $\mathbf{0}$ are independent and Normally distributed. We have

$$\begin{aligned}
\mathcal{L}\Big(\frac{\partial Z_1}{\partial t_1}(\mathbf{0})\Big) &= \mathcal{L}\Big(\frac{\partial Z_1}{\partial t_2}(\mathbf{0})\Big) &= \mathcal{N}(0,\frac{1}{\alpha^2}) \\
\mathcal{L}\Big(\frac{\partial Z_2}{\partial t_1}(\mathbf{0})\Big) &= \mathcal{L}\Big(\frac{\partial Z_2}{\partial t_2}(\mathbf{0})\Big) &= \mathcal{N}(0,\frac{1}{\beta^2}).
\end{aligned}$$

Now define the following random variables:

$$\begin{aligned}
A &= \sqrt{2}\Big(\frac{\partial Z_1}{\partial t_1}(\mathbf{0})+\frac{\beta}{\alpha}\frac{\partial Z_2}{\partial t_2}(\mathbf{0})\Big) & B &= \sqrt{2}\Big(\frac{\partial Z_1}{\partial t_1}(\mathbf{0})-\frac{\beta}{\alpha}\frac{\partial Z_2}{\partial t_2}(\mathbf{0})\Big) \\
C &= \sqrt{2}\Big(\frac{\partial Z_1}{\partial t_2}(\mathbf{0})+\frac{\beta}{\alpha}\frac{\partial Z_2}{\partial t_1}(\mathbf{0})\Big) & D &= \sqrt{2}\Big(\frac{\partial Z_1}{\partial t_2}(\mathbf{0})-\frac{\beta}{\alpha}\frac{\partial Z_2}{\partial t_1}(\mathbf{0})\Big)
\end{aligned}$$

Then

$$\begin{aligned}
\det Z'(\mathbf{0}) &= \frac{\partial Z_1}{\partial t_1}(\mathbf{0})\frac{\partial Z_2}{\partial t_2}(\mathbf{0})-\frac{\partial Z_1}{\partial t_2}(\mathbf{0})\frac{\partial Z_2}{\partial t_1}(\mathbf{0}) \\
&= \frac{\alpha}{2\beta}\Big[(A+B)(A-B)-(C+D)(C-D)\Big] \\
&= \frac{\alpha}{2\beta}\Big[(A^2+D^2)-(B^2+C^2)\Big]
\end{aligned}$$

The variables $R=A^2+D^2$ and $S=B^2+C^2$ are independent and identically Exponentially distributed with rate $\alpha^2/2$. Hence

$$\mathbb{E}\Big(|\det Z'(\mathbf{0})|\Big|Z(\mathbf{0})=\mathbf{0}\Big) \quad = \quad \frac{\alpha}{2\beta}\,\mathbb{E}(|R-S|) \quad = \quad \frac{1}{\alpha\beta}.$$

We now use the above theoretical result to compute an estimate for the intensity of singularities in the tensor field of the fingerprint in Figure 1(a). We then compare the estimated result with the intensity of level two features obtained via visual inspection. We can use sample variograms to estimate the parameters α and β. After interpolating the tensor field on a regular grid and assuming isotropy we obtain the sample variogram for $Z_i, i=1,2$ as

$$\gamma_i(s) \quad = \quad \frac{1}{n(s)}\sum_{||x_k-x_j||}\Big(Z_i(x_k)-Z_i(x_j)\Big)^2$$

where $n(s)$ is the number of grid point pairs (x_k, x_j) that are separated by distance s. Recall that

$$V\Big(Z_1(x) - Z_1(y)\Big) \quad = \quad 2\Big(1 - \exp(-\frac{||x-y||_2^2}{2\alpha^2})\Big)$$

and so we estimate α by fitting a straight line $as + b$ to $-\log(1 - \frac{1}{2}\hat{\gamma}_1(s))$ where $\hat{\gamma}_1(s)$ is the sample variogram of Z_1. Given the fitted slope a our estimate for α is $\hat{\alpha} = 1/\sqrt{2a}$. Using the same estimation procedure for β based on the variogram of Z_2 we obtain as an estimated intensity of zeros for Z:

$$\frac{1}{2\pi\hat{\alpha}\hat{\beta}} \quad = \quad 0.0018.$$

For comparison we manually identified the number of level 2 features in the fingerprint in Figure 1(a). The number of level 2 features per unit area in this fingerprint is 0.0046. While this is roughly of the same order of magnitude, it is somewhat lower than the intensity estimated using the Gaussian model. This is not surprising as not only genuine minutiae will cause singularities in the tensor field but also artifacts such as missed pores or features that were erroneously identified as pores.

8 Conclusions

In this paper we examined a point process observed on an (unobserved) reference structure. We developed a computationally efficient method that estimates a tensor field and so provides local orientation estimates for the underlying reference structure. We illustrated the method on the example of determining local ridge orientation from a pore pattern in a fingerprint. Furthermore, the tensor field provides more information than just a local orientation estimate. Its degenerate points can be related to singularities in the ridge flow pattern, thus providing an explicit relation between pores and minutiae. By assuming a simple Gaussian field we were able to provide an analytic formula for the intensity of level two features. While this paper has focussed on the interesting example of pore patterns from fingerprints, it should be noted that the method is a general tool for the analysis of local anisotropy in point pattern.

References

[1] V. Arsigny, P.Fillard, X. Pennec, and N. Ayache. Log-Euclidean metrics for fast and simple calculus on diffusion tensors. *Magnetic Resonance in Medicine*, 56:411–421, 2006.

[2] David R. Ashbaugh. *Quantitative-Qualitative friction ridge analysis - an introduction to basic and advanced ridgeology.* CRC Press, Boca Raton, 1999.

[3] J-M. Azaïs and M. Wschebor. On the distribution of the maximum of a Gaussian field with d parameters. *The Annals of Applied Probability*, 15:254–278, 2005.

[4] P.G. Batchelor, M. Moakher, D. Atkinson, F. Calamante, and A. Connelly. A rigorous framework for diffusion tensor calculus. *Magnetic Resonance in Medicine*, 53:221–225, 2005.

[5] Thierry Delmarcelle and Lambertus Hesselink. The topology of symmetric, second-order tensor fields. In *IEEE Visualization*, pages 140–147, 1994.

[6] A.K. Jain, Y. Chen, and M. Demirkus. Pores and Ridges: High Resolution Fingerprint Using Level 3 Features. *IEEE Transactions on Pattern Analysis and Machine Intelligence*, 29:15–27, 2007.

[7] R. Mathias and K. Veselić. A relative perturbation bound for positive definite matrices. *Linear Algebra and its applications*, 270:315–321, 1998.

[8] N.R. Parsons, J.Q. Smith, E. Thönnes, L.Wang, and Roland Wilson. Rotationally invariant statistics for examining the evidence from the pores in fingerprints. *Law, Probability and Risk*, 7:1–14, 2008.

[9] A.K. Penttinen and D. Stoyan. Statistical analysis for a class of line segment processes. *Forest Science*, 38:806–824, 1989.

[10] William H. Press, Saul A. Teukolsky, William T. Vetterling, and Brian P. Flannery. *Numerical Recipes with Source Code CD-ROM 3rd Edition: The Art of Scientific Computing*. Cambridge University Press, Cambridge, 2007.

[11] S.O. Rice. Mathematical analysis of random noise. *Bell Systems Technical Journal*, 23:292–332, 1944.

[12] S.O. Rice. Mathematical analysis of random noise. *Bell Systems Technical Journal*, 24:46–156, 1945.

[13] B. Schölkopf, A.J. Smola, and K.R. Müller. Kernel principal component analysis. In *7th International Conference on Artificial Neural Networks, ICANN 97*, volume 1327 of *Springer Lecture Notes in Computer Science*, pages 583–588, Berlin, 1997.

[14] D. Stoyan. Describing the anisotropy of marked planar point processes. *Statistics*, 22:449–462, 1991.

[15] D. Stoyan and V. Beneš. Anisotropy analysis for particle systems. *Journal of Microscopy*, 164:159–168, 1991.

[16] D. Stoyan, W.S. Kendall, and J. Mecke. *Stochastic Geometry and its applications*. Wiley, Chichester, second edition, 1998.

[17] K. Veselić and I. Slapničar. Floating-point perturbations of Hermitian matrices. *Linear Algebra and its applications*, 195:81–116, 1993.

[18] C. Watson. *NIST Special Database 30: Dual Resolution Images from Paired Fingerprint Cards*. National Institute of Standards and Technology, Gaithersburg, MD.